EAI Endorsed Transactions
on Industrial Networks and Intelligent Systems
Research Article EAI.EU

Performance Analysis of NOMA Over $\eta - \mu$ Fading Channels with imperfect SIC

Huu Q. Tran[1,*], Ong Mau Dung[1]

[1]Industrial University of Ho Chi Minh City, Ho Chi Minh City 700000, Vietnam

Abstract

In this paper, a downlink non-orthogonal multiple access (NOMA) network with two users is considered. In particular, the performance of NOMA is evaluated by assuming perfect and imperfect channel state information (CSI). We derive the closed-form expressions for the outage probability over $\eta - \mu$ fading channels in the special case of two users. Moreover, the proposed system model-based NOMA always achieves better performance than that with perfect CSI in the medium SNR region. Monte Carlo simulations are then performed to confirm a good match with the analytical results.

Received on 01 November 2022; accepted on 04 February 2023; published on 11 May 2023

Keywords: $\eta - \mu$ fading channel, outage probability, imperfect SIC.

doi:10.4108/eetinis.v10i1.2833

1. Introduction

There are many challenges in the fifth generation (5G) wireless communication networks and beyond when performing the massive number of connected devices with low delay time, high spectral efficiency, and data rates [1]. To solve these problems, in recent years, non-orthogonal multiple access (NOMA) technology, which many researchers have gained much attention to design communication systems [2]-[4]. NOMA is considered a potential candidate to significantly improve the efficiency spectrum compared to conventional orthogonal multiple access (OMA) [5]. For example, compared to conventional without NOMA, power allocation in NOMA to users which have worse channel conditions is more powerful than users with better channel conditions to guarantee user fairness. NOMA uses superposition coding (SC) signals on the transmitter side, and the receiver side performs successive interference cancellation (SIC). To separate signals, different power levels can be assigned to users at the same time and frequency. In SIC, the signal of a stronger user is decoded and removed first, and then the weaker user decodes its own message [6]. It comes from the benefits of NOMA to improve system performance. For instance, the authors in [7] discussed the advantages and challenges of NOMA for 5G networks. In [8], NOMA for wireless downlink, called multi-tier heterogeneous superposition transmission, is being investigated. In [9], NOMA and OMA, the results showed that NOMA achieves superior energy efficiency in comparison with OMA. Furthermore, [3] also studied the cooperative NOMA, in which BS communicates with the users with weaker channel conditions based on helping relays to decode and forward the signals to others. Thus, establishing reliable communication between the base station and users far away. In order to enhance energy efficiency in NOMA, simultaneous wireless information and power transfer (SWIPT) has been investigated [4], as using stochastic geometry to consider positions of users and radio energy harvesting (EH) at relay to help forwarding the signals to far user. In [2], the authors have considered performance systems to achieve the capacity of the broadcasting channel for the single-antenna downlink NOMA strategy. In [10], the authors have demonstrated MIMO NOMA systems can further provide significant gains compared to OMA schemes. In addition, the uplink and downlink single-cell NOMA communication system wherein multiple users communicate with a single BS with generalized fading channels based on the outage probability (OP) was proposed in [11]. Moreover, the optimal power allocation issue based on average channel state

*Corresponding author. Email: tranquyhuu@iuh.edu.vn

information (CSI) and MIMO-NOMA systems with CSI at the transmitter using ergodic capacity, and OP also was considered in [12]-[13]. However, the works by [12] and [13], are only discussed in cases where the distance between users is predefined. Therefore, most of the existing literature about NOMA requires the knowledge of perfect CSI. In practice, the assumption of perfect CSI in transmitters might be hard to achieve. Furthermore, towards 5G and beyond, there are mobile devices, a number of large users at high-speed, rapidly changing channels, perfect CSI at the transmitter is a challenge. As evident from different aspects, it is necessary to study NOMA users in different 5G-fading realities environments. Therefore, there are many generalized fading models which are used to describe these changing characteristics of the environment, in which the $\eta-\mu$ model is the general model of fading which encompasses propagating in a heterogeneous environment. The OP and sum rate performance of a NOMA downlink system considering $\eta-\mu$ and $\kappa-\mu$ fading channels were studied in [14]. The $\eta-\mu$ fading model inspects a general non-line-of-side propagation strategy by considering two form parameters, η and μ. In [15], the authors have analyzed the OP of the wireless system affected by the $\eta-\mu$ fading and co-channel interference, in an AF relay channel without diversity techniques at the receiver. The outage performance for downlink C-NOMA networks over Nakagami-m fading channels with the imperfect CSI taken into account was investigated in [16]. Moreover, in [17], the authors analyzed the performance of generalized frequency division multiplexing in Rayleigh, Nakagami-m, and Nakagami-q fading channels.

In addition, the connection between Rayleigh and Hoyt distributions that facilitate the analysis of wireless communication systems is considered in [18]. Motivated by these constraint conditions, we investigate the use of partial CSI, which reduces the complexity of the system and enhances the spectral efficiency of NOMA in practice.

In this paper, we consider a downlink NOMA network, where the base station and users are equipped with a single antenna. We also assume the channel estimation error model, where the BS and the users perform the channel estimation and predict the variance of the estimation error. For performance evaluation, we also carried out the expressions of OP over $\eta-\mu$ fading channels.

The rest of the paper is organized as follows. Section 2 presents the system model and channel characteristics. Section 3 analysis of the outage performance and the system throughput of NOMA schemes with perfect and imperfect CSI. In Section 4, numerical results are shown and Monte Carlo simulations are performed to verify the theoretical analysis. Finally, Section 5 concludes the paper.

2. System model and channel characteristics

2.1. System model

It can be seen from Fig. 1, the system includes a single antenna source (S) that serves two NOMA users at the downlink. We have h_1 and h_2, respectively, characterize link BS-user D_1 and link BS-user D_2. Two users, D_1 and D_2, are facilitated with half-duplex (HD) mode. During EH time αT, in which T is the block time and α is the fraction of the block time allocated for EH, and its condition is $0 \leq \alpha < 1$. The harvested energy, E_{D_i} is given by

$$E_{D_i} = \upsilon P_S \alpha |h_i|^2, i \in \{1, 2\} \tag{1}$$

where P_S depicts the normalized transmission power at the source (S), υ is the energy conversion efficiency. Depending on the quality of EH electric circuitry $0 < \upsilon < 1$. From obtained E_{D_i} in (1), the transmitted power from node S, P_{D_i} is given by

$$\begin{aligned} P_{D_i} &= E_{D_i} \big/ (1-\alpha)\, T \\ &= \upsilon P_S \alpha |h_i|^2 \big/ (1-\alpha)\, T \end{aligned} \tag{2}$$

The received signal at D_1 and D_2, respectively, are given by

$$y_1 = h_1 \sqrt{P_S} \left(\sum_{j=1}^{2} \sqrt{v_j} x_j \right) + \omega_1, \tag{3}$$

$$y_2 = h_2 \sqrt{P_S} \left(\sum_{j=1}^{2} \sqrt{v_j} x_j \right) + \omega_2, \tag{4}$$

where ω_1 and ω_2 depicts the additive white Gaussian noise (AWGN) with zero mean and variance of N_0 at the D_1, and D_2, respectively, and x_j is assumed to be normalized the unity power signal for the $j-th$ user, i.e., $\mathrm{E}\left\{x_j^2\right\} = 1$ where $\mathrm{E}\{\}$ is the expectation operator. The $j-th$ user's power allocation factor v_j satisfies the relationship $v_2 > v_1$ with $\sum_{j=1}^{2} \sqrt{v_j} = 1$, which is for the fairness of users. In the first phase, the signal-to-interference-plus-noise ratio after treating x_1 as interference can be computed by

$$\Gamma_{D_1, x_2} = \frac{v_2 \rho_S |h_1|^2}{v_1 \rho_S |h_1|^2 + 1} = \frac{v_2 \rho_S \gamma_1}{v_1 \rho_S \gamma_1 + 1}, \tag{5}$$

where $\gamma_i \triangleq |h_i|^2, i \in \{1, 2\}$ and the transmit signal-to-noise ratio (SNR) is determined at the S as $\rho_S = P_S / N_0$. Note that γ_1 and γ_2 are independent random variables (RVs).

It should be noted that imperfect SIC (ipSIC) occurs, and the SINR to detect x_2 is given as

$$\Gamma_{D_1, x_1}^{\text{ipSIC}} = \frac{v_1 \rho_S \gamma_1}{\rho_S |h_I|^2 + 1}, \tag{6}$$

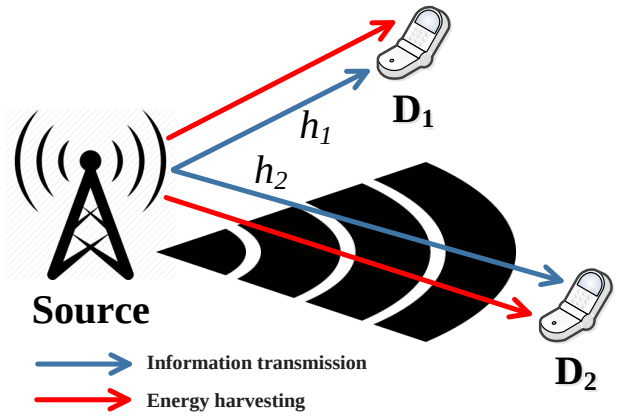

Figure 1. System model.

where $|h_I|^2 \sim CN(0, \lambda_I)$ in with $\lambda_I (0 \leq \lambda_I \leq 1)$ describes the residual interference level caused by ipSIC and $CN \sim (a, b)$ complex normal distribution with average a and variance b.
Similarly, the instantaneous SINR at D_2 for detecting x_2 is given by

$$\Gamma_{D_2,x_2} = \frac{v_1 \rho_S \gamma_2}{v_2 \rho_S \gamma_2 + 1}, \tag{7}$$

2.2. Channel Characteristics

The probability density function (PDF) of $\gamma = \gamma_1 = \gamma_2$ is given by [15, $Eq.(1)$]

$$f_\gamma(x) = \frac{2\sqrt{\pi}\mu^{\mu-0.5} h^\mu x^{\mu-0.5}}{\Gamma(\mu) H^{\mu-0.5} \overline{\gamma}^{\mu-0.5}} e^{-\frac{2\mu h}{\overline{\gamma}} x} \times I_{\mu-0.5}\left(\frac{2\mu H}{\overline{\gamma}} x\right), \tag{8}$$

Where $\Gamma(x)$ is the Gamma function, $I_z()$ is the modified Bessel function of the first kind, $\overline{\gamma} = \mathrm{E}\{\gamma\}$, μ is related to the fading severity, $h = \left(2 + \eta^{-1} + \eta\right)/4$ and $H = \left(\eta^{-1} + \eta\right)/4$ with $0 < \eta < \infty$. For arbitrary values of μ. According to [16, $Eq.(2)$] the cumulative distribution functions (CDF) of γ can be determined by

$$F_\gamma(x) = \frac{(\Lambda_1 \Lambda_2)^\mu}{\Gamma(1+2\mu)} x^{2\mu} \times \Phi_2(\mu, \mu; 1 + 2\mu; -\Lambda_1 x, \Lambda_2 x), \tag{9}$$

where $\Phi_2 \equiv \Phi_2^{(2)}$ is the confluent Lauricella function [20], $\Lambda_1 = \frac{2\mu(h-H)}{\overline{\gamma}}$ and $\Lambda_2 = \frac{2\mu(h+H)}{\overline{\gamma}}$. For integer values of μ and with the help of [19, $Eq.(15)$] and [21, $Eq.(8.352.6)$] , $F_\gamma(x)$ can be greatly simplified

$$F_{|h|^2}(x) = \frac{\sqrt{\pi}}{\Gamma(\mu)} \sum_{k=0}^{\infty} \frac{H^{2j} \Gamma(2(\mu+k))}{k! \Gamma(\mu+k+0.5) 2^{2(\mu+k)-1} h^{\mu+2k}} \times \left[1 - e^{-2\mu h x} \sum_{m=0}^{2(\mu+k)-1} \frac{(2\mu h)^m x^m}{m!}\right], \tag{10}$$

Next, we have PDF and CDF of $|h_I|^2$ are given by

$$f_{|h_I|^2}(x) = \frac{1}{\lambda_I} e^{-\frac{x}{\lambda_I}}, \tag{11}$$

and

$$F_{|h_I|^2}(x) = 1 - e^{-\frac{x}{\lambda_I}}, \tag{12}$$

3. Analysis of outage probability and system throughput

3.1. Outage probability

First, the OP of D_1 is calculated as

$$\begin{aligned} \mathrm{OP}_1 &= 1 - \Pr\left(\Gamma_{D_1,x_2} > \varepsilon_2, \Gamma_{D_1,x_1}^{\mathrm{ipSIC}} > \varepsilon_1\right) \\ &= 1 - \Pr\left(\gamma_1 > \delta_2, \gamma_1 > \delta_1\left(\rho_S |h_I|^2 + 1\right)\right), \end{aligned} \tag{13}$$

where $\varepsilon_i = 2^{\frac{R_i}{1-\alpha}} - 1$, R_i is the target rate at $D_i (i = 1, 2)$, $\delta_2 = \frac{\varepsilon_2}{\rho_S(v_2 - v_1 \varepsilon_2)}$ and $\delta_1 = \frac{\varepsilon_1}{v_1 \rho_S}$.
Then, P_1 can be calculated by

$$\begin{aligned} \mathrm{OP}_1 &= 1 - \Pr\left(\gamma_1 > \delta_1\left(\rho_S |h_I|^2 + 1\right)\right) \\ &= 1 - \int_0^\infty f_{|h_I|^2}(x) \left[1 - F_{\gamma_1}(\delta_1(\rho_S x + 1))\right] dx, \end{aligned} \tag{14}$$

Case 1: when $\mu \in \mathbb{N}, \forall \mu \geq 0$ then we use PDF of (11) and CDF of (10), (14) is given by

$$\begin{aligned} \mathrm{OP}_1 &= 1 - \int_0^{\infty} f_{|h_I|^2}(x)\left[1 - F_{\gamma_1}\left(\delta_1\left(\rho_S x + 1\right)\right)\right] dx \\ &= \frac{\sqrt{\pi}}{\Gamma(\mu)} \sum_{k=0}^{\infty} \frac{H^{2j}\Gamma(2(\mu+k))}{k!\Gamma(\mu+k+0.5)2^{2(\mu+k)-1}h^{\mu+2k}} \\ &\times \left[\begin{array}{l} 1 - \frac{e^{-2\mu h\delta_1}}{\lambda_I} \sum\limits_{m=0}^{2(\mu+k)-1} \frac{(2\mu h\delta_1)^m}{m!} \\ \times \int_0^{\infty} e^{-\left(\frac{1}{\lambda_I} + 2\mu h\delta_1\rho_S\right)x} (\rho_S x + 1)^m dx \end{array} \right], \end{aligned} \tag{15}$$

Using [21, $Eq.$(1.111)] and [21, $Eq.$(3.351.3), OP_1 is given by

$$\begin{aligned} \mathrm{OP}_1 &= \frac{\sqrt{\pi}}{\Gamma(\mu)} \sum_{k=0}^{\infty} \frac{H^{2j}\Gamma(2(\mu+k))}{k!\Gamma(\mu+k+0.5)2^{2(\mu+k)-1}h^{\mu+2k}} \\ &\times \left[\begin{array}{l} 1 - e^{-2\mu h\delta_1} \\ \times \sum\limits_{m=0}^{2(\mu+k)-1} \sum\limits_{r=0}^{m} \binom{m}{r} \frac{r!(2\mu h\delta_1)^m \lambda_I^r \rho_S^r}{m!(1+2\lambda_I\mu h\delta_1\rho_S)^{r+1}} \end{array} \right], \end{aligned} \tag{16}$$

Case 2: when $\mu \in \mathrm{I}, \forall \mu \geq 0$ then we use PDF of (10) and CDF of (9), (14) can be given by

$$\begin{aligned} \mathrm{OP}_1 &= \frac{(\Lambda_1\Lambda_2)^{\mu}\delta_1^{2\mu}}{\Gamma(1+2\mu)\lambda_I} \\ &\times \int_0^{\infty} \left[\begin{array}{l} e^{-\frac{x}{\lambda_I}} (\rho_S x + 1)^{2\mu} \\ \times \Phi_2\left(\begin{array}{l} \mu, \mu; 1+2\mu; \\ -\Lambda_1\delta_1\left(\rho_S x + 1\right), \\ \Lambda_2\delta_1\left(\rho_S x + 1\right) \end{array} \right) \end{array} \right] dx, \end{aligned} \tag{17}$$

Specifically, we set $q = \frac{x}{\lambda_I}$ with the help of Gauss-Laguerre integration in [21, $Eq.$(25.4.45). The closed-form approximation of the OP_1 at D_1 is given by

$$\begin{aligned} \mathrm{OP}_1 &\approx \frac{(\Lambda_1\Lambda_2)^{\mu}\delta_1^{2\mu}}{\Gamma(1+2\mu)} \sum_{n=1}^{N} \chi_n \Theta(q_n)^{2\mu} \\ &\times \Phi_2\left(\mu, \mu; 1+2\mu; -\Lambda_1\delta_1\Theta\left(q_n\right), -\Lambda_2\delta_1\Theta\left(q_n\right)\right), \end{aligned} \tag{18}$$

where $\Theta\left(q_n\right) = \left(\rho_S\lambda_I q + 1\right)$, χ_n and q_n are the weight and abscissas for the Gauss-Laguerre integration, respectively. More specifically, q_n is the $n-th$ zero of Laguerre polynomial $L_N\left(q_n\right)$ and the corresponding the n-th weight is given by $\chi_n = \frac{(N!)^2 q_n}{\left[L_{N+1}(q_n)\right]^2}$. The parameter N is to ensure a complexity-accuracy trade off. Finally, the OP at D_2 is calculated as

$$\begin{aligned} \mathrm{OP}_2 &= 1 - \Pr\left(\Gamma_{D_2, x_2} > \varepsilon_2\right) \\ &= 1 - \Pr\left(\gamma_2 > \delta_2\right) = F_{\gamma_2}\left(\delta_2\right), \end{aligned} \tag{19}$$

Case 1: when $\mu \in \mathbb{N}, \forall \mu \geq 0$ then we use CDF of (10), (19) is given by

$$\begin{aligned} \mathrm{OP}_2 &= \frac{\sqrt{\pi}}{\Gamma(\mu)} \sum_{k=0}^{\infty} \frac{H^{2j}\Gamma(2(\mu+k))}{k!\Gamma(\mu+k+0.5)2^{2(\mu+k)-1}h^{\mu+2k}} \\ &\times \left[1 - e^{-2\mu h\delta_2} \sum_{m=0}^{2(\mu+k)-1} \frac{(2\mu h\delta_2)^m}{m!}\right]. \end{aligned} \tag{20}$$

Case 2: when $\mu \in \mathrm{I}, \forall \mu \geq 0$ then we use CDF of (9), (19) is given by

$$\mathrm{OP}_2 = \frac{(\Lambda_1\Lambda_2)^{\mu}\delta_2^{2\mu}}{\Gamma(1+2\mu)} \Phi_2\left(\begin{array}{l} \mu, \mu; 1+2\mu; \\ -\Lambda_1\delta_2, -\Lambda_2\delta_2 \end{array} \right), \tag{21}$$

3.2. System Throughput

With a given constant R, the transmitted information of the source node depends on the OP performance due to wireless fading channels. Therefore, the system throughput is determined by

$$\begin{aligned} \tau_{D_1} &= \frac{(1-\mathrm{OP}_1)R_1(1-\alpha)T/2}{T} \\ &= \frac{(1-\mathrm{OP}_1)R_1(1-\alpha)}{2}, \end{aligned} \tag{22}$$

Where OP_1 is given in (14)-(16).

$$\tau_{D_2} = \frac{(1-\mathrm{OP}_2)R_2(1-\alpha)}{2}, \tag{23}$$

where OP_2 is given in (19)-(21).

4. NUMERICAL RESULTS

The Monte-Carlo simulation results from an average of over 10^7 independent channel realizations. Target data rates at D_1 and D_2 are $R_1 = 1$ (BPCU) and $R_2 = 0.5$ (BPCU), respectively. Mean values of the interference signal channel power gains $\lambda_I = -30\,(\mathrm{dB})$. The power allocation coefficients $v_1 = 0.2$ and $v_2 = 0.8$. The Gauss Laguerre quadratures have several points, $N = 40$.

Figure 2 plots the OP versus SNR according to different fair values of η and μ. The figures show that the curves of the OP for User 2 decrease quickly while that for User 1 decrease gradually. In SNR range of from 40 to 60 dB, the OP for User 1 is almost constant. The OP of User 1 is always higher than that for User 2. For effects of η on the OP, the figure shows that the lower the η, the higher the OP. On contrary, the higher the μ, the lower the OP. The OP for ipSIC only decreases in a certain range of SNR, e.g., herein from 0 to 40 dB, then tends to keep a constant value.

Figure 3 plots the OP versus SNR according to perfect SIC and ipSIC. One can see from the figure that the OP curves for both users in case of perfect SIC decrease linearly in the SNR range of from 20 to 60 dB. The OP for user 2 is always lower than that for user 1, regardless

of the variation of SNR. When the ipSIC occurs, the OP curves of user 1 generate inflection points and tend to decrease gradually in the SNR range from 0 to 40 dB. However, these OP curves are almost constant when SNR increases from 40 to 60 dB. The higher the λ, the higher the OP for ipSIC. We can conclude that the ipSIC considerably impacts on the OP.

Figure 4 plots the OP versus power allocation coefficient v_1 of from 0 to 0.5 in cases of perfect and ipSIC. The figure shows that the OP for user 1 decreases in the v_1 range of from 0 to 0.35 and then increases in the v_1 range, from 0.35 to 0.5, while that for user 2 is always an increase in the overall v_1 range. Therefore, as an obvious results, the OP for two users exists some intersection points. On the left side of the intersection, the OP of the user 2 is significantly lower than that of user 1. On the contrary, this OP at the right side of the intersection points tends to coincide with each other. Besides, the OP for ipSIC is always the highest. It can be concluded that an ipSIC can cause negative impacts on the OP. In addition, the simulations also consider the different transmitting power, such as 10, 15 and 20 dB, respectively. The OP for both users increases when the transmitting power P_S decreases. This is due to the fact that the stronger the transmitting signal, the better the quality of the signal. We can observe from figure 5 that the OP for user 2 is lower than that for user 1. The OP for ipSIC is always higher than that for perfect SIC. Besides, when the transmitting power decreases, the OP increases in the overall target rate range. Moreover, the OP for both users increases highly and is asymptotic to 1 when the target rate increases. Specifically, in this work, the OP for user 1 reaches 1 when the target rate is equal to 2. The OP for user 2 reaches 1 when the target rate is equal to 2.25.

Fig. 6 plots the system throughput according to different values of power allocation factor v_2. We can see from this figure that the system throughput of user 1 in the case of perfect CSI is higher than imperfect CSI and both cases decrease when increasing v_2 from 0.55 to 0.95. The throughput of user 1 is larger than that of user 2 with the values of v_2 $(0.5, 0.75)$ in the case perfect CSI and v_2 $(0.5, 0.8)$ in the case imperfect CSI. However, the system throughput of user 2 reaches saturation when increasing the values of v_2. It can be explained that the SNR at user 2 used to detect x_1 and x_2 is higher than the minimum value of SNR at user 1 used to detect x_2.

Figure 7 describes the throughput versus transmitting SNR ρ (dB) with different values λ_I. From the figure, it is shown that the throughput of user 1 with perfect SIC is considerably higher than that with ipSIC when increasing ρ (dB) about $(10 \div 30)$ dB. Additionally, when decreasing the residual interference level caused by ipSIC (λ_I), the throughput of user 1 is increasing. Moreover, at medium transmit SNR about $(0 \div 20)$ dB, the throughput of user 2 is higher than that for user 1.

5. Conclusion

In this paper, we have studied the OP and the throughput of NOMA schemes for the two users. The numerical derivations of NOMA protocols in two cases with perfect and imperfect CSI. The analytical evaluations of NOMA protocols based on perfect CSI at medium SNR always outperforms NOMA with imperfect CSI. In addition, the outage performance of user 1 is always higher than that for user 2. The results shows that the η lower, the outage performance is higher. On the contrary, the higher μ, OP is lower. Moreover, the analytical expressions showed that the ipSIC considerably impacts on the OP and the system throughput.

Data Availability

The data used to support the findings of this study are included in the paper.

Conflicts of Interest

The authors declare there is no conflict of interest in this manuscript.

Acknowledgement

This study was self-funded by the authors.

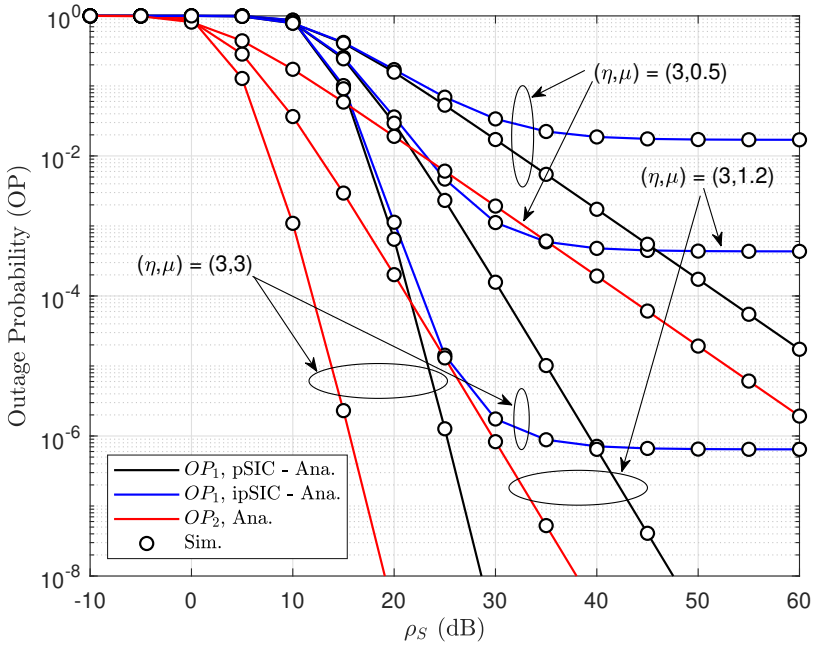

Figure 2. Outage probability versus SNR according to different value fairs of η and μ.

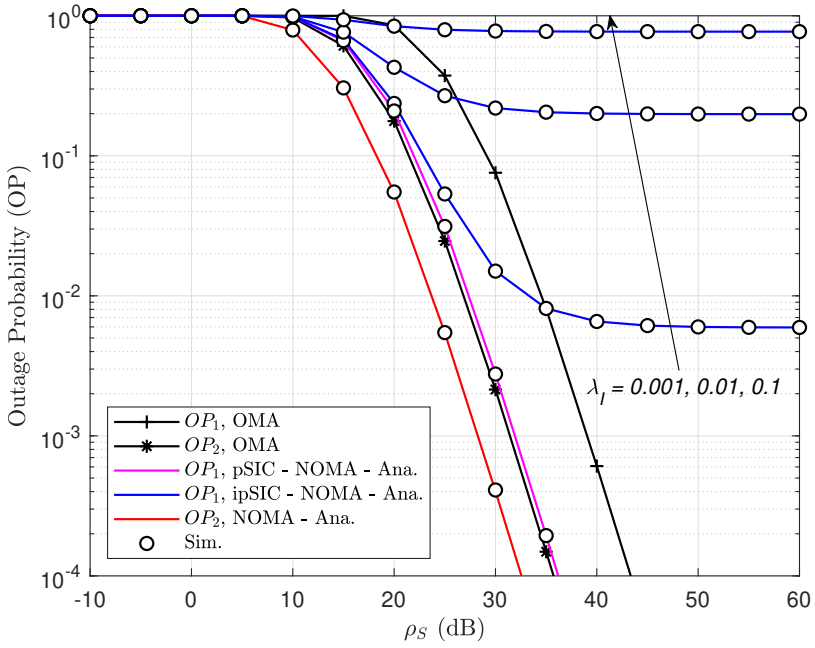

Figure 3. Outage probability versus SNR with $R_1 = 1.5\,(BPCU), R_2 = 1\,(BPCU), \eta = 0.1$ and $\mu = 1.2$.

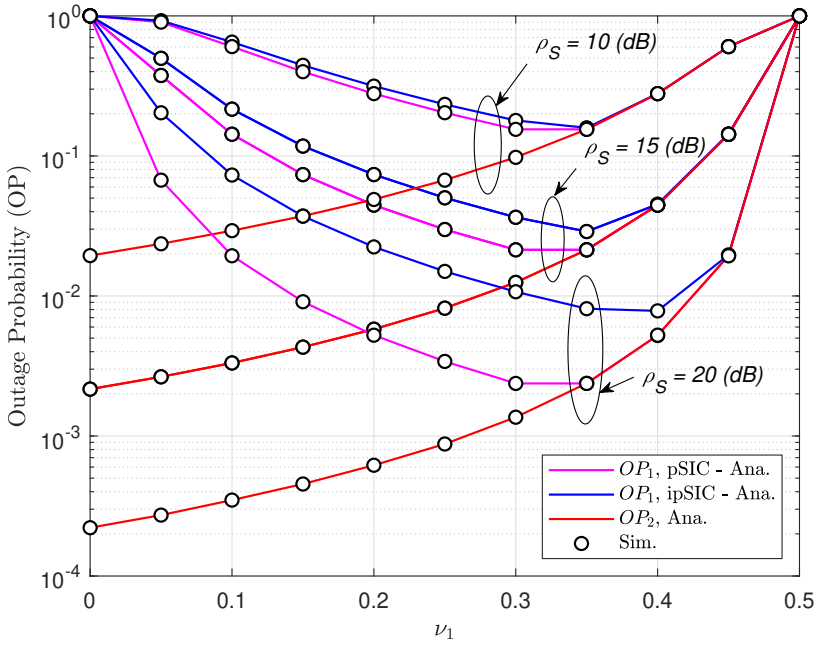

Figure 4. Outage probability versus power allocation coefficient v_1 with $\lambda_I = -20\,(\text{dB})$, $R_1 = R_2 = 0.5\,(BPCU)$, $\eta = 0.5$ and $\mu = 1$.

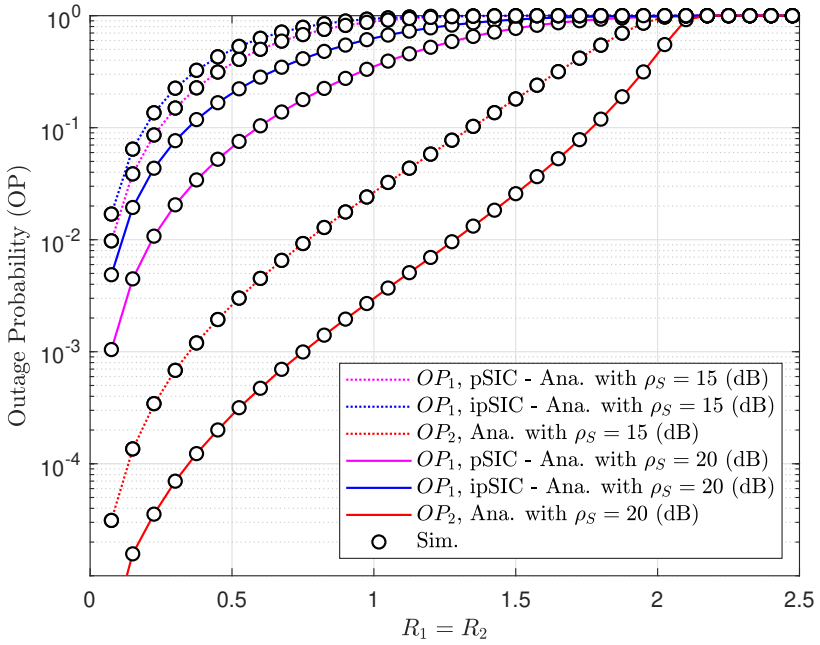

Figure 5. Outage probability versus target rate and different values of P_S with $v_1 = 0.05, v_2 = 0.95, \eta = 0.5$ and $\mu = 1$.

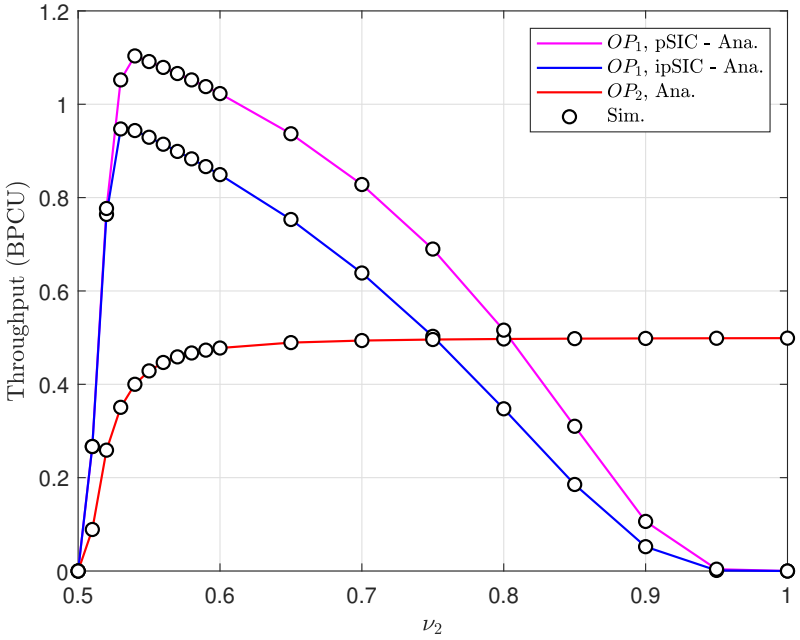

Figure 6. System throughput versus v_2 with $\lambda_I = -20\,(\text{dB})$, ρ=15 (dB), $R_1 = 1.5\,(BPCU)$, $R_2 = 0.5\,(BPCU)$, $\eta = 0.5$, and $\mu = 1$.

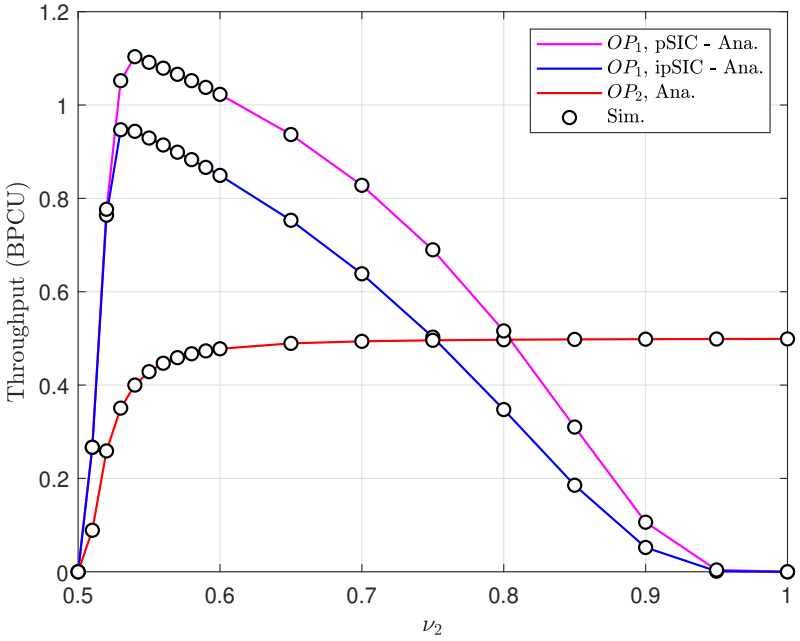

Figure 7. System throughput versus ρ with $v_1 = 0.05, v_2 = 0.95, \eta = 0.5$, and $\mu = 1$.

References

[1] L. U. Khan, I. Yaqoob, M. Imran, Z. Han and C. S. Hong, "6G Wireless Systems: A Vision, Architectural Elements, and Future Directions," IEEE Access, vol. 8, pp. 147029-147044, Aug. 2020.

[2] D. Wan, M. Wen, F. Ji, H. Yu and F. Chen,"Non-Orthogonal Multiple Access for Cooperative Communications: Challenges, Opportunities, and Trends," IEEE Wireless Communications, vol. 25, no. 2, pp. 109-117, Apr. 2018.

[3] Liaqat, Mahrukh, Kamarul Ariffin Noordin, Tarik Abdul Latef, and Kaharudin Dimyati,"Power-domain non orthogonal multiple access (PD-NOMA) in cooperative networks: an overview," Wireless Networks, vol. 25, no. 1, pp. 181-203, Jan. 2020.

[4] Huu Q. Tran, Tien-Tung Nguyen, Ca V. Phan, and Quoc-Tuan Vien,"Power-splitting relaying protocol for wireless energy harvesting and information processing in NOMA systems," IET Communications, vol. 13, no. 14, pp. 2132-2140, Aug. 2019.

[5] Huu Q. Tran, Ca V. Phan, and Quoc-Tuan Vien,"Power splitting versus time switching based cooperative relaying protocols for SWIPT in NOMA systems," Physical Communication, vol. 41, pp. 1010981-101113, Aug. 2020.

[6] Z. Ding, X. Lei, G. K. Karagiannidis, R. Schober, J. Yuan and V. K. Bhargava,"A Survey on Non-Orthogonal Multiple Access for 5G Networks: Research Challenges and Future Trends," IEEE Journal on Selected Areas in Communications, vol. 35, no. 10, pp. 2181-2195, Oct. 2017.

[7] Mathur, H., Deepa, T. ,"A Survey on Advanced Multiple Access Techniques for 5G and Beyond Wireless Communications," Wireless Pers Commun, vol. 118, pp. 1775-1792, May. 2021.

[8] Huu Q. Tran, Ca V. Phan, and Quoc-Tuan Vien,"Optimizing energy efficiency for supporting near-cloud access region of UAV based NOMA networks in IoT systems," Wireless Communications and Mobile Computing, vol. 2021, pp. 1-12, Oct. 2021.

[9] Huu Q. Tran, Ca V. Phan, and Quoc-Tuan Vien,"Performance analysis of power-splitting relaying protocol in SWIPT based cooperative NOMA systems," EURASIP Journal on Wireless Communications and Networking, pp.110-136, Apr. 2021.

[10] S. H. Amin, A. H. Mehana, S. S. Soliman and Y. A. Fahmy,"Power Allocation for Maximum MIMO-NOMA System User-Rate," IEEE Globecom Workshops (GC Wkshps), Abu Dhabi, United Arab Emirates, Dec. 2018, pp. 1-6.

[11] A. Agarwal, R. Chaurasiya, S. Rai and A. K. Jagannatham,"Outage Probability Analysis for NOMA Downlink and Uplink Communication Systems With Generalized Fading Channels," IEEE Access, vol. 8, pp. 220461-220481, Dec. 2020.

[12] S. Timotheou and I. Krikidis,"Fairness for Non-Orthogonal Multiple Access in 5G Systems," IEEE Signal Processing Letters, vol. 22, no. 10, pp. 1647-1651, Oct. 2015.

[13] Q. Sun, S. Han, C. -L. I and Z. Pan,"On the Ergodic Capacity of MIMO NOMA Systems," IEEE Wireless Communications Letters, vol. 4, no. 4, pp. 405-408, Aug. 2015.

[14] P. Sharma, A. Kumar, and M. Bansal,"Performance analysis of downlink NOMA over $\eta - \mu$ and $\kappa - \mu$ fading channels," IET Commun., vol. 14, no. 3, pp. 522-531, Feb. 2020.

[15] Konicanin, S., Vasic, S., Milic, D., Petrovic, N., & Suljovic, S,"Outage Probability of the Dual-Hop AF Relay Transmission System in the $\eta - \mu$ Fading Channel," 28th Telecommunications Forum (TELFOR), Nov. 2020, pp. 1-4.

[16] J. Men, J. Ge and C. Zhang,"Performance Analysis for Downlink Relaying Aided Non-Orthogonal Multiple Access Networks With Imperfect CSI Over Nakagami- m Fading," IEEE Access, vol. 5, pp. 998-1004, 2017.

[17] Shravan Kumar Bandari, Satyendra Singh Yadav, V.V. Mani,"Analysis of GFDM in generalized $\eta - \mu$ fading channel: A simple probability density function approach for beyond 5G wireless applications," AEU - International Journal of Electronics and Communications, pp. 154260-154284, vol. 153, Aug. 2022.

[18] J. M. Romero-Jerez and F. J. Lopez-Martinez,"A New Framework for the Performance Analysis of Wireless Communications Under Hoyt (Nakagami-q) Fading," IEEE Transactions on Information Theory, vol. 63, no. 3, pp. 1693-1702, Mar. 2017.

[19] Suresh Kumar Balam, P. Siddaiah, Srinivas Nallagonda,"Optimization analysis of cooperative spectrum sensing system over generalized $\kappa - \mu$ and $\eta - \mu$ fading channels," Wireless Personal Communications, no. 4, pp. 1-20, Oct. 2020.

[20] E. Martos-Naya, J. M. Romero-Jerez, F. J. Lopez-Martinez and J. F. Paris,"A MATLAB program for the computation of the confluent hypergeometric function Φ_2," Repositorio Institucional Universidad de Malaga RIUMA., Tech. Rep, pp. 1-3, Sep. 2016.

[21] Gradshteyn, I.S., Ryzhik, I.M,"Table of integrals, series and products," *Academic, San Diego, CA, 7th edn*, 2007.